Simulations of Serpentine Plasma Actuators in a Laminar Boundary Layer

Mark Riherd* and Subrata Roy†

Applied Physics Research Group, University of Florida, Gainesville, FL, 32608

Laminar simulations of a boundary layer with plasma actuation have been performed. The addition of plasma actuation to the boundary layer introduces streamwise vorticity to the flow. This streamwise vorticity is shown to impact the boundary layer thicknesses, as well as introduce significant spanwise variations in the velocity field. The general flow structure is examined, and qualitatively comparisons with the quiescent results of the existing literature. The angle of the vectored jet generated by this actuator geometry is found to increase as the magnitude of the plasma actuation is increased. The levels of streamwise vorticity and circulation due to the addition of the serpentine actuation are also measured.

Nomenclature

u, v, w	Flow velocities
p	Pressure
U, V, W	Contravariation velocities
x, y, z	Spatial coordinate system
ξ, η, ζ	Non-dimension, body fitted coordinate system
τ	Shear stress
E	Energy
T	Temperature
Q	Heat flux
$\mathbf{Q}$	Dependent variables
$\mathbf{S}$	Source variable
$\mathbf{F}, \mathbf{G}, \mathbf{H},$	Inviscid fluxes
$\mathbf{F_v}, \mathbf{G_v}, \mathbf{H_v},$	Viscid fluxes
$\mathcal{J}$	Grid Jacobian
ω_x	Streamwise vorticity
$\bar{u}, \bar{v}, \bar{w}$	Spanwise averaged flow velocities
$\bar{\omega}_x$	Spanwise averaged streamwise vorticity
u', v', w'	Spanwise variations in the flow velocities (i.e.$u' = u - \bar{u}$)
ω_x	Spanwise variations in the streamwise vorticity
u_∞	Freestream velocity
u_p	Induced velocity
$\delta_{99\%}$	Boundary layer height
δ^*	Displacement boundary layer height
θ	Momentum boundary layer height
Re	Reynolds number
D_c	Non-dimensional body force magnitude
M_∞	Mach number
Pr	Prandtl number

*Graduate Research Assistant, Student Member AIAA.

†Associate Professor, Associate Fellow AIAA

γ	Velocity ratio
I	Integrated value
σ	Standard deviation
ϕ	General variable
Subscript	
i	direction
x_i	differentiated in the x_i^{th} direction

I. Introduction

Boundary layer control is one aspect of fluid dynamics that is becoming increasingly more important as the need for energy efficient aircraft increases.[1] If effective, control of laminar and turbulent boundary layers can lead to decreased levels of viscous surface drag and form drag due to flow separation.

A wide number of actuators exist for flow control applications,[2] but one of particular usefulness is the dielectric barrier discharge (DBD) actuator. This type of actuator is able to impart momentum to a localized volume of fluid through a electrodynamic body force.[3–5] Furthermore, this class of devices have the advantages of being surface compliant, having a near instantaneous response to an input voltage, and a high bandwidth of application, as well as being able to be duty cycled, allowing them to be implemented as components of active and passive flow control systems. One concern with in applying these actuators is that they have relatively low control authority, as they can only accelerate a quiescent fluid to velocities of 8 to 10 m/s.

These actuators have seen significant application both experimentally and in numerical simulations for separation control for airfoils,[6–8] turbine blades,[9] and general separated boundary layers.[10,11] The effects of applying these actuators in boundary layers has also been examined. In particular, there have also been efforts to use these actuators to control the laminar to turbulent transitions in boundary layers,[12–14] and multiple destabilizing effects have been theorized.[15]

The geometry of these actuators can also be easily modified in order to produce a specific perturbations to the flow. By modifying the electrode geometries, configurations such as the Plasma Synthetic Jet Actuator (PSJA),[16] the horseshoe geometry actuator,[17,18] and the serpentine geometry actuator.[18] The geometry relevant to the present work is the serpentine geometry, which is a generalized class of actuator geometries.[18–20] This type of actuator geometry is able to introduce three dimensional vortical effects to a flow. These three-dimensional vortical effects are hypothesized to improve the control authority of the actuators for transition control applications where the acceleration of the transition process is desired,[7,21] though no experiments have yet been performed to verify this hypothesis.

The aim of this study is to help develop an understanding and to quantify certain flow modifications that occur as serpentine plasma actuation is applied to a boundary layer. Recent studies have examined the qualitative effects of these flows, but quantitative parametric studies are still lacking in the literature. Quantitative measurements of the changes in boundary layer height, the velocity fields downstream of the plasma actuation, and the levels of circulation in the boundary layer would help to provide good comparisons between this class of plasma actuators and other flow control devices when trying to take advantage of specific boundary layer control mechanisms.

II. Numerical Methods

In order to simulate these flows, the Implicit Large Eddy Simulation (ILES) Navier-Stokes solver, FDL3DI[22] is employed. This code solves the compressible two-dimensional Navier-Stokes equations in a body fitted diagonalized, conservation form.

$$\frac{\partial \mathbf{Q}}{\partial t} + \frac{\partial}{\partial \xi}\left(\mathbf{F} - \frac{1}{Re}\mathbf{F}_v\right) + \frac{\partial}{\partial \eta}\left(\mathbf{G} - \frac{1}{Re}\mathbf{G}_v\right) + \frac{\partial}{\partial \zeta}\left(\mathbf{H} - \frac{1}{Re}\mathbf{H}_v\right) = D_c\mathbf{S} \tag{1}$$

The dependent variables are defined as

$$\mathbf{Q} = \frac{1}{\mathcal{J}}\left[\begin{array}{ccccc} \rho, & \rho u, & \rho v, & \rho w, & \rho E \end{array}\right]^T \tag{2}$$

with the inviscid and viscid fluxes are defined as

$$\mathbf{F} = \frac{1}{\mathcal{J}} \begin{bmatrix} \rho U \\ \rho u U + \xi_x p \\ \rho v U + \xi_y p \\ \rho w U + \xi_z p \\ \rho E U + \xi_{x_i} u_i p \end{bmatrix}, \ \mathbf{G} = \frac{1}{\mathcal{J}} \begin{bmatrix} \rho V \\ \rho u V + \eta_x p \\ \rho v V + \eta_y p \\ \rho w V + \eta_z p \\ \rho E V + \eta_{x_i} u_i p \end{bmatrix}, \ \mathbf{H} = \frac{1}{\mathcal{J}} \begin{bmatrix} \rho W \\ \rho u W V + \zeta_x p \\ \rho v W + \zeta_y p \\ \rho w W + \zeta_z p \\ \rho E W + \zeta_{x_i} u_i p \end{bmatrix} \tag{3}$$

$$\mathbf{F_v} = \frac{1}{\mathcal{J}} \begin{bmatrix} 0 \\ \xi_{x_i} \tau_{i1} \\ \xi_{x_i} \tau_{i2} \\ \xi_{x_i} \tau_{i3} \\ \xi_{x_i} (u_j \tau_{ij} - Q_i) \end{bmatrix}, \ \mathbf{G_v} = \frac{1}{\mathcal{J}} \begin{bmatrix} 0 \\ \eta_{x_i} \tau_{i1} \\ \eta_{x_i} \tau_{i2} \\ \eta_{x_i} \tau_{i3} \\ \eta_{x_i} (u_j \tau_{ij} - Q_i) \end{bmatrix}, \ \mathbf{H_v} = \frac{1}{\mathcal{J}} \begin{bmatrix} 0 \\ \zeta_{x_i} \tau_{i1} \\ \zeta_{x_i} \tau_{i2} \\ \zeta_{x_i} \tau_{i3} \\ \zeta_{x_i} (u_j \tau_{ij} - Q_i) \end{bmatrix}, \tag{4}$$

and the right hand side source term are defined as

$$\mathbf{S} = \frac{1}{\mathcal{J}} \begin{bmatrix} 0, & f_x, & f_y, & f_z, & u_i f_{x_i} \end{bmatrix}^T \tag{5}$$

where

$$E = \frac{T}{\gamma(\gamma - 1) M_\infty^2} + \frac{1}{2}(u^2 + v^2 + w^2) \tag{6}$$

$$Q_i = -\left(\frac{1}{(\gamma - 1) M_\infty^2} \right) \left(\frac{\mu}{Pr} \right) \frac{\partial \xi_j}{\partial x_i} \frac{\partial T}{\partial x i_j} \tag{7}$$

$$\tau_{ij} = \mu \left(\frac{\partial \xi_k}{\partial x_j} \frac{\partial u_i}{\partial x i_k} + \frac{\partial \xi_k}{\partial x_i} \frac{\partial u_i}{\partial x i_k} - \frac{2}{3} \delta_{ij} \frac{\partial \xi_l}{\partial x_k} \frac{\partial u_k}{\partial x i_l} \right) \tag{8}$$

$$U = \frac{\partial \xi}{\partial x_i} u_i, \ V = \frac{\partial \eta}{\partial x_i} u_i, W = \frac{\partial \zeta}{\partial x_i} u_i \tag{9}$$

In this system of equations, ρ represents the fluid density, u and v are the flow velocities, p is pressure, and E is the specific energy. All of these variables are non-dimensionalized by their reference values. Pressure is the exception to this, as it has been non-dimensionalized by the dynamic head ($\rho_\infty u_\infty^2$). τ_{ij} represents the stress tensor and Q_i is the heat flux vector. f_x, f_y and f_z describe the normalized, spatially varying body force. The magnitude of this body force is modulated by the value of D_c. ξ, η, and ζ represent the body fitted coordinate system, $\mathcal{J}$ is the grid Jacobian, U,V and W are the body fitted velocities. The non-dimensional variables Re, Pr, and Ma_∞ represent the Reynolds, Prandtl, and Mach number, respectively. Here, γ represents the ratio of specific heats and is equal to 1.4. The ideal gas law is also used in order to close the system of equations. While this is the compressible form of the Navier-Stokes equations, and incompressible flow can be solved by setting the Mach number, M_∞, to an appropriately low value. It has been determined that a value of $M_\infty = 0.1$ provides a reasonable balance of incompressibility and numerical stability. At this Mach number, variations to the fluid density are less than 1% throughout the domain. Temperature (and viscosity via Sutherland's law) variations are similarly small.

The grid used for these simulations is a non-uniform Cartesian mesh with $763 \times 151 \times 65$ ($x \times y \times z$) grid points spanning the domain $[0.3, 8.0] \times [0, 1.5] \times [0, 0.1]$, as can be seen in Fig. 1. This mesh is densest near the region of the serpentine plasma actuator on the surface of the wall. The mesh becomes less dense as one approaches the far field and downstream boundaries. Geometric stretching of the mesh is employed in order to ensure a smooth variation in mesh density. The stretching of the mesh downstream prevents reflections off of the boundary, but reduces the domain from which results can be drawn. The mesh stretching begins at $x = 5.0$, allowing for the flow to develop after the inlet. The region of $x \in [0.5, 4.0]$ provides sufficient resolution for data extraction. Upstream of the plasma actuator, a Blasius boundary layer is used as the inflow condition, where the leading edge of the plate would be placed at $x = 0$. For the far field, and downstream of the actuator, no shear conditions are applied in order to allow for the development of the boundary layer. Periodic boundary conditions are used in the spanwise direction.

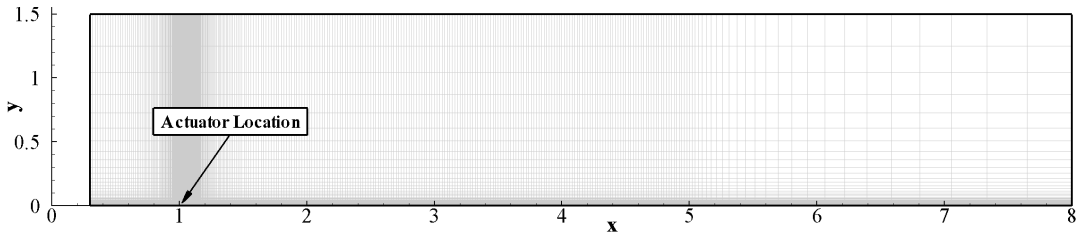

Figure 1. Side view of the computational mesh used. Every other grid point is shown.

A. Body Force Model

The body force is implemented through the use of the right hand side source term, **S**. This spatially varying term is described by the use of a plasma body force model. While there are a number of models in existence, with varying degrees of complexity and accuracy,[23–26] a phenomenological model[27] has been selected for use in this study, as it possesses a good balance of physical behavior and ease of implementation. An example of the serpentine geometry can be seen in Fig. 2.

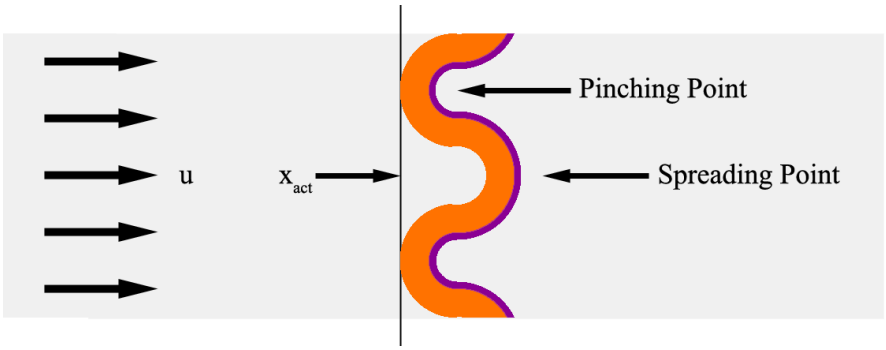

Figure 2. Top view of the serpentine geometry actuator.

For a free stream Reynolds number of $Re_x = 50,000$, the (non-dimensional) displacement boundary layer height, δ^*, is =0.00769. The plasma actuator has a spanwise wavelength of 0.1. This indicates that the spanwise wavenumber of this flow is $\beta = 0.440$.

The magnitude of the plasma actuation is the primary parameter of interest in the present study, which is characterized by the maximum velocity the (non-serpentine) plasma actuator is able to generate under quiescent conditions. Using this description of the problem, the focus remains on the fluidic effects, reducing the emphasis of effects away from specific actuator geometries and operating parameters.

In order to determine the value of D_c, necessary to produce a plasma with a specific velocity, two-dimensional simulations run on a comparable mesh as the three-dimensional simulations were performed. In these simulations, a body force representing a standard geometry (linear, straight electrodes) plasma actuator is introduced to quiescent fluid. After a sufficient amount of time, the maximum velocity at a specific downstream location of the actuator reaches a steady value. This value is defined as u_p. In order to ensure that this value is relevant to the free stream velocity, the non-dimensional velocity ratio,

$$\gamma = \frac{u_p}{u_\infty} \tag{10}$$

is used to characterize the relative magnitude of the plasma actuation.

III. Results

A number of simulations have been performed in order to examine the effects of a serpentine geometry actuator in a laminar boundary layer. These simulations are based around flow conditions at relatively low

Reynolds numbers, where the actuator is placed at a streamwise Reynolds number of $Re_x = 50,000$. These simulations are not perturbed in any active manner, other than the steady addition of momentum to the flow through the plasma body force. Even so, some unsteady behavior and oscillations are noted downstream of the point $x = 1.8$. These unsteady variations suggest that the flow is unstable, the reasons for which will be discussed. Previous simulations[19] and experiments[20] of serpentine geometry actuators indicate that the flow is highly unsteady, so the introduction of strong instabilities to a boundary layer flow are not entirely unexpected. Upstream and for a short distance downstream of the actuator, the unsteadiness is minimal, and the flow should be considered a well behaved laminar flow.

A. Primary flow features

There are two primary flow features in the flow that has been modified with the use of a serpentine geometry plasma actuator. The first of these is the forcing of fluid away from the surface in the region immediately downstream of the actuator in a vectored jet, comparable to the effects of a plasma synthetic jet.[16] Evidence of this effect can be found in Fig. 3a, c, and e. The second of these, is the counter rotating streamwise oriented vortices that propagate downstream,[18,20] evidence of which are given in Figs. 5 and 6b, d, and f. Both of these effects have been previously reported in the existing literature.[18–20] In addition to these flow features, there is an interesting second velocity local velocity maximum that has been noticed at the impingement plane, downstream of the plasma actuator under quiescent conditions. This effect is also noticed in the current simulations, though only when the velocities generated by the plasma actuator are comparable to the free stream velocity ($\gamma \approx 0.75$).

Examining the flow field at the impingement point of the actuator (Fig. 3a,c,e, and g), it can be seen that the vectored jet produced in the presence of a mean flow is of much shallower angle than that produced under quiescent conditions. The angle of the jet is strongly dependent on the magnitude of the plasma actuation, where a larger velocity ratio produces a steeper jet. At the spreading point (Fig. 3b,d,f, and h), fluid is pulled down, towards the surface, an effect that has been seen for standard geometry plasma actuators in boundary layers previously. Overall, based on the spanwise averaged velocity field, the effect of the vectored jet is minimal, indicating that it is a localized effect.

Counter rotating vortices are a common occurrence when studying the transition of flows, and have been identified as the temporally most amplified modes in boundary layers and channel flows.[28] In transitional flows, the counter-rotating vortices are accompanied by periodic streaks of fast and slow moving fluid between the vortices, indicating that the vortices are transporting high momentum fluid into and low momentum fluid out of the boundary layer region. The streamwise velocity variations are usually one to two orders of magnitude larger than the wall normal or spanwise velocity components, and are believed to be a major contributor to the laminar to turbulent transition process. Upon examination of the serpentine plasma actuated boundary layer, it is found that the streamwise velocity variations (Fig. 6a, c, and e) qualitatively match those responsible for a certain transition process in the boundary layer, including the large difference between the streamwise and wall normal/spanwise velocity components. The structures present here do not appear to be the optimal structures compared to those described by previous researchers for the Blasius boundary layer.[28] They are in roughly the right position in the boundary layer, but the shape of the streamwise vortical structures have a much more complex shape. The linearly growing optimal streamwise vortex consists of only a single vortical structure, where the streamwise vortical structures generated by the serpentine geometry plasma actuator have multiple smaller streamwise vortices attached, though they do quickly decay as they develop downstream. However, as the spanwise perturbations develop in the streamwise direction, the non-optimal components appear to damp themselves out, resulting in a spanwise variation which better agrees with the optimal perturbation. Even so, this type of behavior in the flow suggests that the serpentine plasma actuator should be very adept at initiating the transition process in boundary layers.

The magnitude and centroid of these velocity and vorticity can both be quantified. For clarity, the integrated value of these effects will done using the standard deviation (σ) of these quantities across the span of the actuator, such that the total effect and centroid are defined as

$$I_u = \int_0^\infty \sigma_u dy \tag{11a}$$

$$I_{\omega_x} = \int_0^\infty \sigma_{\omega_x} dy \tag{11b}$$

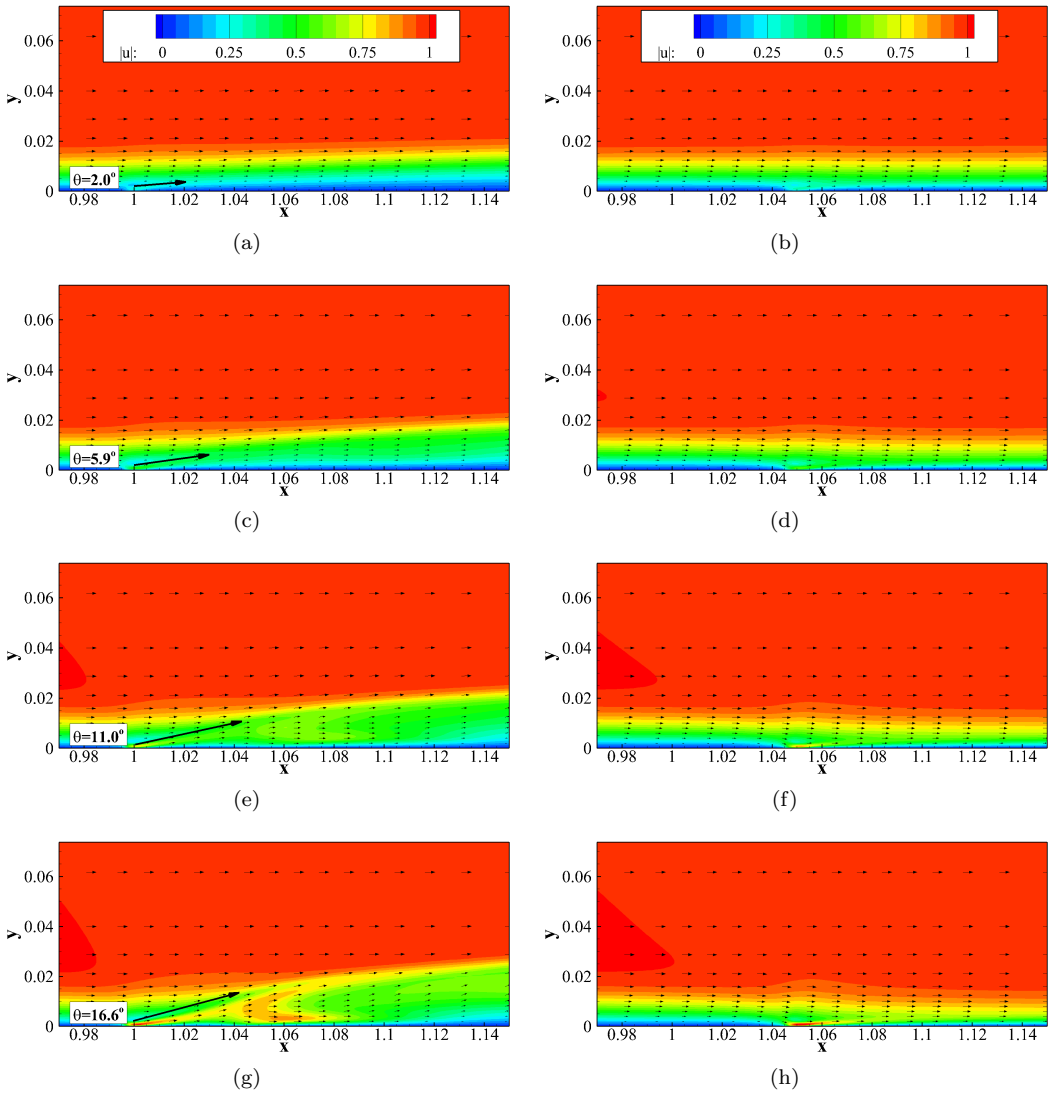

Figure 3. Comparisons of the velocity field near the plasma actuator for the cases (a,b) $\gamma = 0.25$, (c,d) $\gamma = 0.50$, (e,f) $\gamma = 0.75$, and (g,h) $\gamma = 1.00$, at the (a,c,e,g) impingement point and (b,d,f,h) spreading point. For the vectors, every tenth vector in the x and y directions are shown. The angle of the vectored jet is also indicated by the larger black arrow.

$$y_u = \frac{\int_0^\infty y\sigma_u dy}{\int_0^\infty \sigma_\phi dy} \tag{12a}$$

$$y_{\omega_x} = \frac{\int_0^\infty y\sigma_{\omega_x} dy}{\int_0^\infty \sigma_\phi dy} \tag{12b}$$

Comparisons of these metrics are show in Fig.7a and b. In reviewing these results, it can be seen that total variation across the span of the streamwise vorticity scales nicely with the velocity ratio of the plasma actuation, γ. The total variation across the span of the streamwise velocity only seems to scale very close to the actuator ($x_{act} = 1.0$). Farther downstream, the values do not match up as well. The data suggests that there may be some non-linear saturation point, which upon reaching the flow cannot sustain additional growth of spanwise velocity variations. The variations in the behavior of the total spanwise variation of the streamwise velocity can likely be attributed to the movement of the streamwise vortices away from the surface. The streamwise vorticity transports high momentum fluid into the boundary layer and lower momentum fluid out of it, and into the free stream. As the vortices move away from the surface, the momentum difference in the fluid being transported into and out of the boundary layer will decrease. This

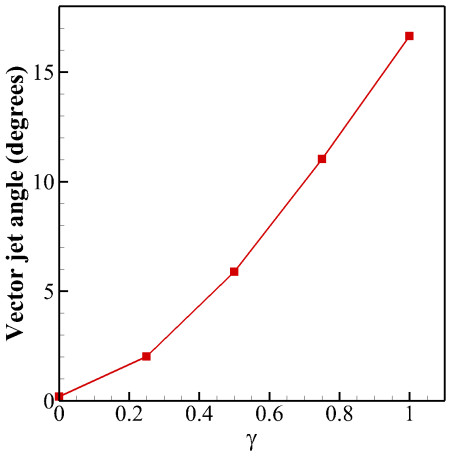

Figure 4. Angle of the vectored jet as the velocity ratio is varied. This angle was measured as the maximum flow angle at the height of $y = \delta_0^* = 0.0079$ along the impingement plane.

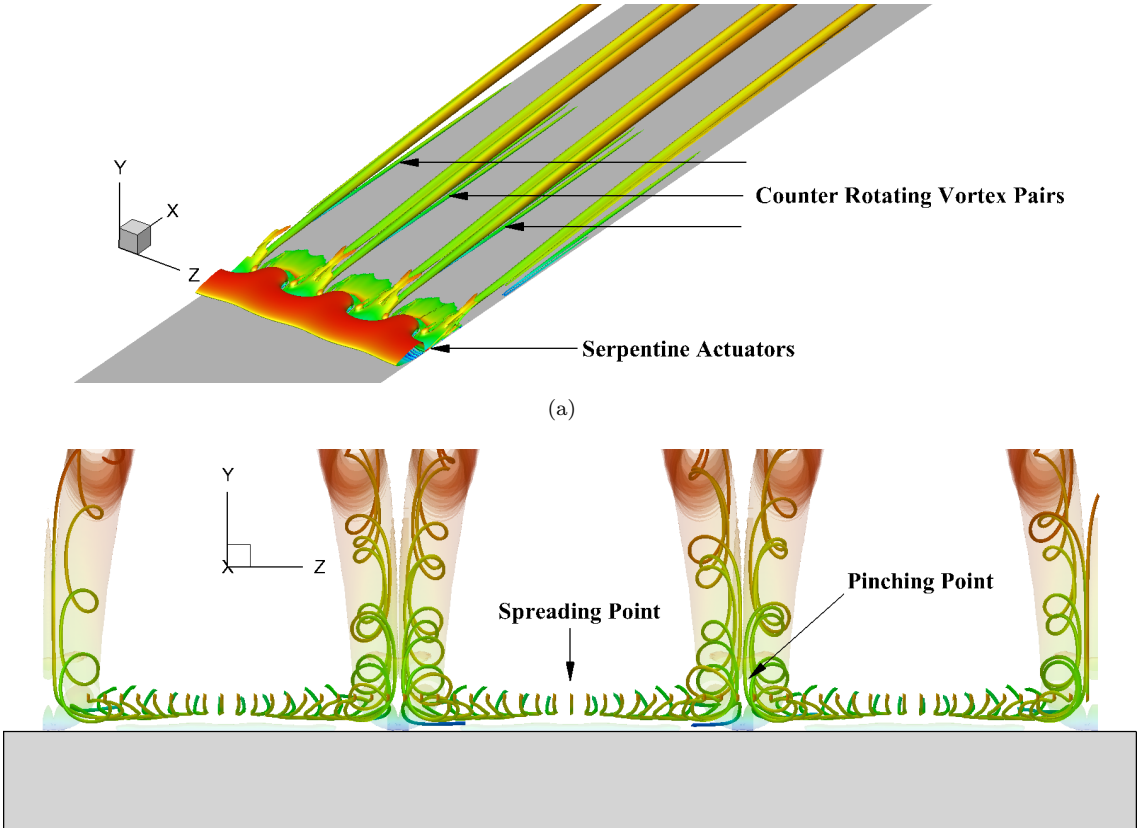

Figure 5. (a) Q-criteria (colored by velocity magnitude) and (b) streamtraces (with translucent Q-criteria) for the case of $\gamma = 1.00$. The data set is repeated twice in the z-direction, only a single wavelength was simulated.

decrease in momentum transport will thus lead to a decreased rate at which the spanwise variation in the streamwise velocity grows. While this is all occurring, the spanwise variation in the streamwise velocity will decay, as any wake does. These two competing effects determine the magnitude of the streamwise velocity variation. Should the velocity ratio be sufficiently small, these effects could potentially be linear in nature farther downstream of the actuator. It appears that for velocity ratios as large as those tested at present,

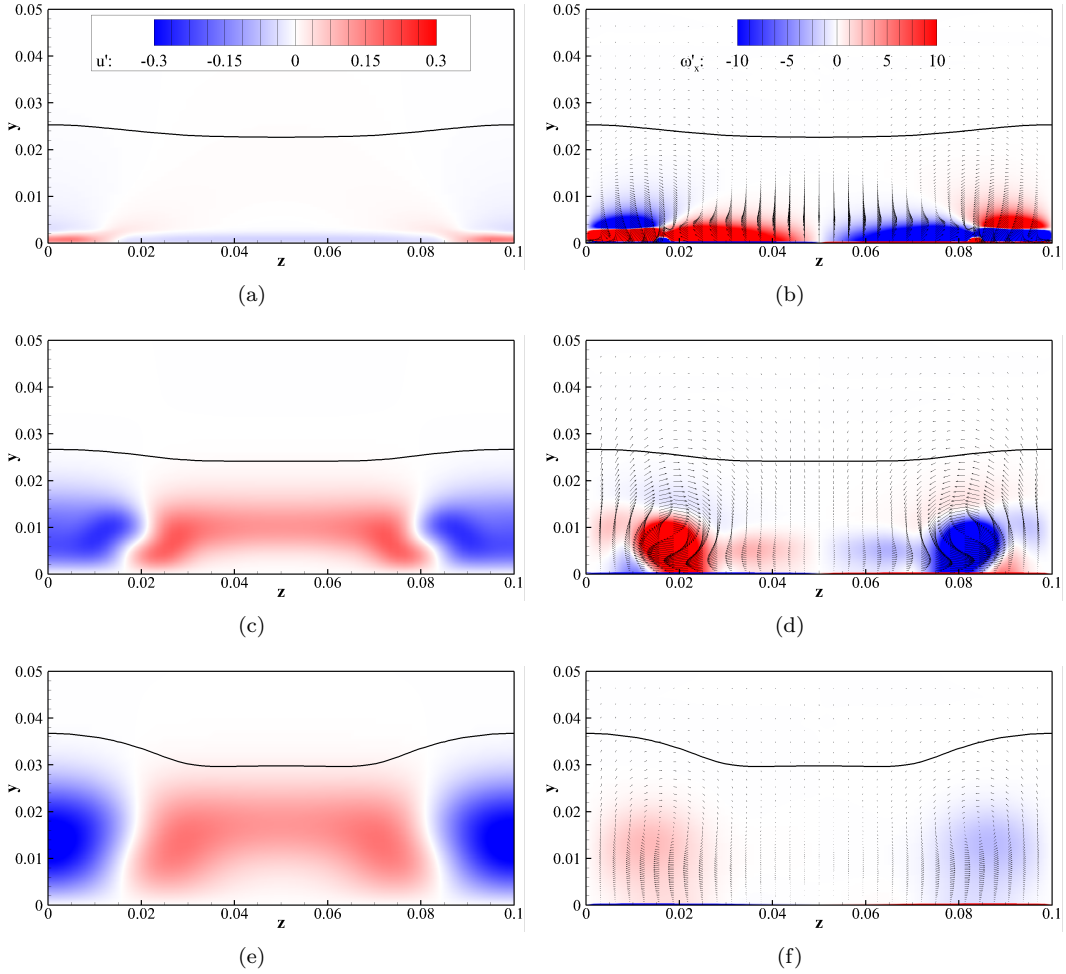

Figure 6. Streamwise variations in the velocity magnitudes (a,c,e) and streamwise vorticity and velocity vectors (b,d,f) at x=1.0 (a,b), 1.2 (c,d), and 1.9 (e,f) for the case of $Re_x = 50,000$ and $\gamma = 0.25$. The 99% boundary layer height ($\delta_{99\%}$) is marked by the thick solid line.

the effects are non-linear.

B. Modifications to the boundary layer heights

The addition of serpentine actuation produces some significant changes to the boundary layer. Upstream of the plasma actuation, the boundary layer heights match those of the analytical Blasius solution. In the region near the actuator, and downstream of it, spanwise variations in the flow velocity lead to spanwise variations in the boundary layer heights. The spanwise average and standard deviations of the boundary layer heights can be found in Fig. 8. For the 99% boundary layer, it seems that the average height of the boundary layer increases with the level of plasma actuation, a behavior also seen for the momentum thickness boundary layer. For the displacement thickness boundary layer, the opposite appears to be true, as this value appears to decrease as the level of plasma actuation is increased. For all of these boundary layer heights, the spanwise variations increase with the magnitude of the plasma actuation, which is consistent with the other calculations of the spanwise variations.

These changes in the boundary layer thicknesses should be attributed to the streamwise vortical structures. These vortical structures are raising the boundary layer heights along the impingement plane, while lowering it in the spreading plane. For the displacement and momentum boundary layers, the addition of momentum back into the boundary layer would indicate a fuller profile. This fuller profile leads to the reduction in the displacement boundary layer height. At the same time, the addition of momentum near the surface, may lead to an increse in surface drag. This change in surface drag then leads to an increase in the

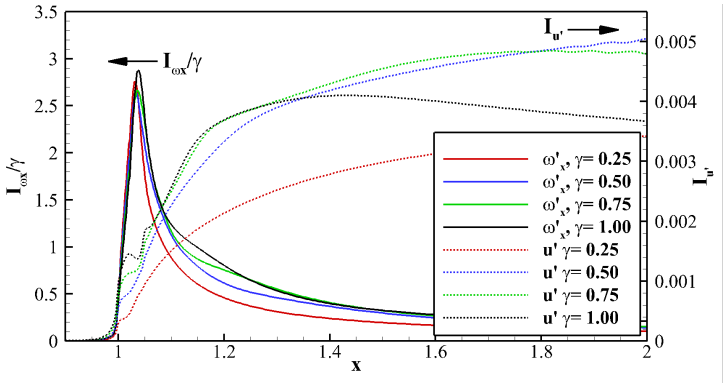

(a)

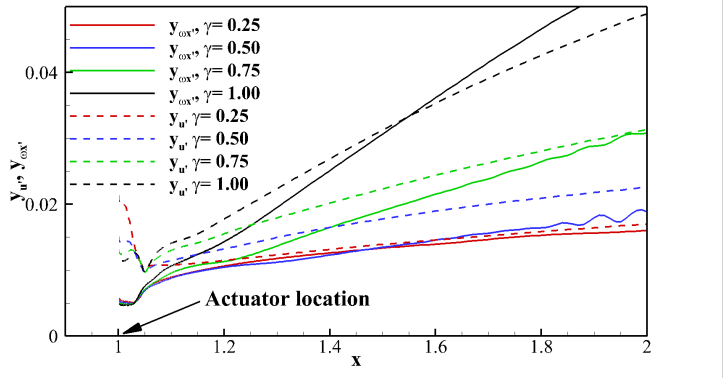

(b)

Figure 7. (a) Integrated values of the spanwise variations of ω_x' and u' for varying velocity ratios. (b) Centroids of the spanwise variations of ω_x' and u'.

streamwise derivative of the momentum boundary layer ($d\theta/dx$), which can cause the momentum thickness boundary layer to increase.

IV. Conclusions

From these simulations, quantitative characterization of the serpentine geometry plasma actuators in a laminar boundary is available. The structures in the flow have been examined as a function of the magnitude of the plasma actuation, characterized by the velocity ratio of the plasma actuation. Effects previously described in the existing literature have been quantified through parametric studies.

Many of the changes in the flow can be attributed to the introduction of streamwise oriented vortices into the boundary layer by the serpentine geometry actuation. These structures transport high momentum fluid into the boundary layer, while moving lower momentum fluid out of it. Because of these structures, there is additional mixing of fluid in the boundary layer, as well as changes to the boundary layer heights and surface friction.

In the past, streamwise vortical structures have been connected to the laminar to turbulent transition process in a number of shear flows.[28] A particular feature of these transition inducing, streamwise vorticies is that they include significant streamwise velocity variations across the span of the boundary layer, where the streamwise velocity variations are one to two orders of magnitude larger than the spanwise or wall normal velocity variations. The results of the present simulations indicate that the streamwise vortical structures generated by serpentine plasma actuation are comparable to those which lead to the transition of laminar flow including the effects on the variations in velocity. This indicates that there is a strong potential for these devices to be used for accelerating the transition process.

Near the actuator, the addition of serpentine geometry plasma actuation has been shown to generate a

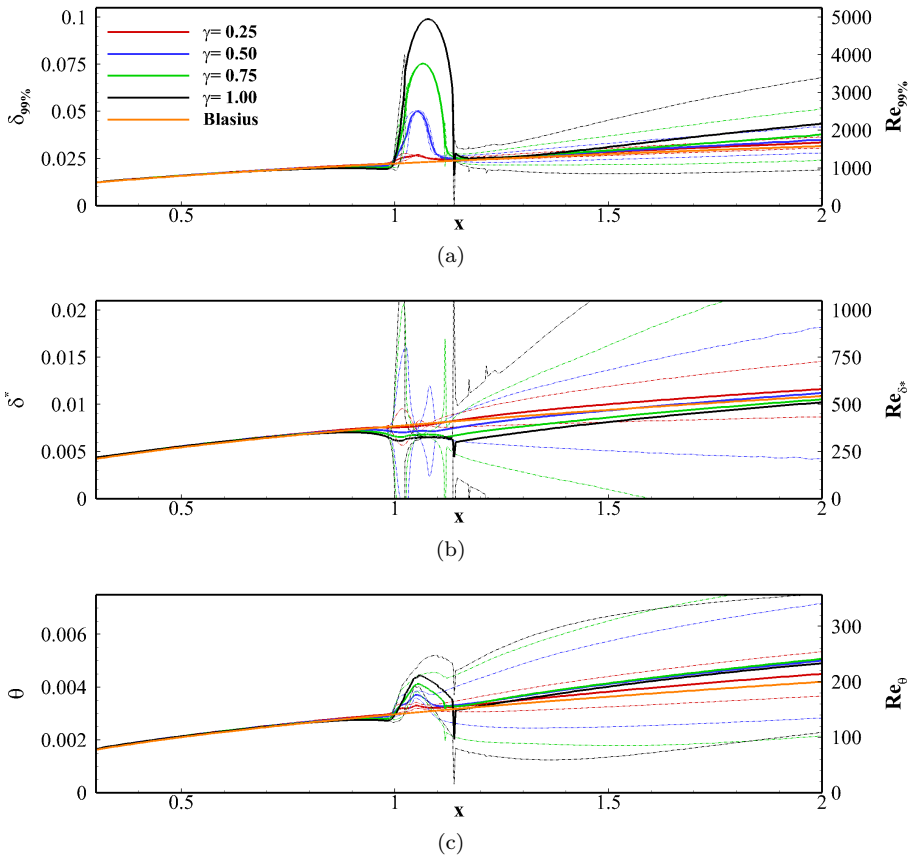

Figure 8. Comparison of the average (a) 99%, (b) displacement, and (c) momentum thickness boundary layer heights (solid lines) and their spanwise standard deviations (dashed lines) as a function of the velocity ratio with the Blasius boundary layer solution.

vectored jet of fluid moving away from the wall. As this flow feature is located immediately downstream of the plasma actuation, the streamwise vortical structure and spanwise velocity variations will be directly affected by it. The angle of this vectored jet is dependent on the ratio of the induced velocity by the plasma actuation and the free stream velocity. Further studies should help to clarify how this vectored jet is dependent on the velocity ratio of u_p/u_∞ as well as other parameters, such as the amount of wall normal momentum at the pinching point under quiescent conditions for the actuation. Just as u_p has been calibrated for varying values of D_c, the wall normal momentum and the vectored jet angle at the pinching point need to be calibrated based on the actuator geometry and magnitude of plasma actuation under quiescent conditions. Based this additional data, it may be possible to generate physics based approximations of the vectored jet and other flow properties, which could then be used to better implement these actuators in flow control applications. For example, in high speed flows, a linearization (i.e. for small values of γ) of the flow field may be possible with respect to γ, from which control strategies could be developed.

Better understanding of these actuators under quiescent and bulk flow conditions should lead to more focused application of these devices. In particular, these devices show potential as an active trip for initiating the laminar to turbulent transition process. The ability of these actuator to be turned on and off (unlike discrete roughness elements) as well as to be flush mounted (unlike synthetic jets) suggest that serpentine geometry plasma actuators could be an optimal flow control device for this application, especially when the flow conditions are likely to be varied.

Acknowledgments

The authors would like to thank Dr. Miguel Visbal and the Computational Sciences Branch of the Air Force Research Laboratory's Air Vehicles Directorate for the use of their code, FDL3DI. The first author

was supported by the University of Florida Graduate School Fellowship Award.

References

[1]Anders, S. G., III, W. L. S., , and Washburn, A. E., "Active Flow Control Activities at NASA Langley," *42th AIAA Aerospace Sciences Meeting, AIAA-2004-2623*, 2010.

[2]Cattafesta, L. N. and Sheplak, M., "Actuators for Active Flow Control," *Annual Review of Fluid Mechanics*, Vol. 43, 2011, pp. 247–272.

[3]Roth, J. R., Sherman, D. M., and Wilkinson, S. P., "Electrohydrodynamic Flow Control with a Glow-Discharge Surface Plasma," *AIAA Journal*, Vol. 38, 2000, pp. 1166–1172.

[4]Corke, T. C., Enloe, C. L., and Wilkinson, S. P., "Dielectric Barrier Discharge Plasma Actuators for Flow Control," *Annual Review of Fluid Mech.*, Vol. 66, 2010, pp. 505–529.

[5]Moreau, E., "Airflow control by non-thermal plasma actuators," *Journal of Physics D: Applied Physics*, Vol. 40, 2007, pp. 605–636.

[6]Post, M. L. and Corke, T. C., "Separation Control on High Angle of Attach Airfoil Using Plasma Actuators," *AIAA Journal*, Vol. 42, No. 11, 2004, pp. 2177–2184.

[7]Rizzetta, D. P. and Visbal, M. R., "Numerical Investigation of Plasma-Based Control for Low-Reynolds-Number Airfoil Flows," *AIAA Journal*, Vol. 49, No. 2, 2011, pp. 411–425.

[8]Gaitonde, D. V., Visbal, M., and Roy, S., "A coupled approach for plasma-based flow control simulations of wing-sections," *44th AIAA Aerospace Sciences Meeting*, 2006.

[9]Rizzetta, D. P. and Visbal, M. R., "Numerical Investigation of Plasma-Based Flow Control for Transitional Highly Loaded Low-Pressure Turbine," *AIAA Journal*, Vol. 45, No. 10, 2007, pp. 2554–2564.

[10]Rizzetta, D. P. and Visbal, M. R., "Large-Eddy Simulation of Plasma-Based Turbulent Boundary-Layer Separation Control," *AIAA Journal*, Vol. 48, No. 12, 2010, pp. 2793–2810.

[11]Schatzman, D. M. and Thomas, F. O., "Turbulent Boundary Layer Separation Control with Plasma Actuators," *AIAA Paper 2008-4199*, 2008.

[12]Grundmann, S. and Tropea, C., "Active Cancellation of artificially induced Tollmien-Schlichting waves using plasma actuators," *Exp. in Fluids*, Vol. 44, 2008, pp. 795–806.

[13]Grundmann, S. and Tropea, C., "Experimental damping of boundary-layer oscillations using DBD plasma actuators," *Intl. J. of Heat and Fluid Flow*, Vol. 30, 2009, pp. 394–402.

[14]Duchmann, A., Kurz, A., Widmann, A., Grundmann, S., and Tropea, C., "Characterization of Tollmien-Schlichting Wave Dampting by DBD Plasma Actuators Using Phase-Locked PIV," *50th AIAA Aerospace Sciences Meeting*, 2012.

[15]Riherd, M. and Roy, S., "Linear Stability Analysis of a Boundary Layer with Plasma Actuators," *50th AIAA Aerospace Sciences Meeting*, 2012.

[16]Santhanakrishnan, A. and Jacob, J. D., "Flow control with plasma synthetic jet actuators," *Journal of Physics D: Applied Physics*, Vol. 40, No. 3, 2007, pp. 637.

[17]Wang, C. C. and Roy, S., "Electrodynamic Enhancement of Film Cooling of Turbine Blades," *Journal of Applied Physics*, Vol. 104, 2008.

[18]Roy, S. and Wang, C. C., "Bulk flow modification with horseshoe and serpentine plasma actuators," *Journal of Physics D: Applied Physics*, Vol. 42, 2009.

[19]Wang, C., Durscher, R., and Roy, S., "Three-dimensional effects of curved plasma actuators in quiescent air," *Journal of Applied Physics*, Vol. 109, 2011.

[20]Durscher, R. and Roy, S., "Three-dimensional flow measurements induced from serpentine plasma actuators in quiescent air," *Journal of Physics D: Applied Physics*, Vol. 45, 2012.

[21]Riherd, M. and Roy, S., "A Comparison of Linear and Serpentine Geometry Plasma Actuation for Controlling a Transitionally Separated Airfoil Flow," *Third Annual FCAAP Symposium and Exhibition, Tallahassee, FL, April 26-27*, 2012.

[22]Rizzeta, D. P., Visbal, M. R., and Morgan, P. E., "A high-order compact finite-difference scheme for large-eddy simulations of active flow control," *Prog. in Aerospace Sci.*, Vol. 44, 2008, pp. 397–426.

[23]Singh, K. P. and Roy, S., "Force approximation for a plasma actuator operating in atmospheric air," *Journal of Applied Physics*, Vol. 103, 2008.

[24]Maden, I., Kreigsei, J., Maduta, R., Jakilrić, S., Grundmann, S., and Tropea, C., "Derivation of a Plasma-Actuator Model Utilizing Quiescent-Air PIV Data," *20th Annual Conference of the CFD Community of Canada, Canmore, May9-12*, 2012.

[25]Boeuf, J. P., Lagmich, Y., Unfer, T., Callegar, T., and Pitchford, L. C., "Electrohydrodynamic force in dielectric barrier discharge plasma actuators," *Journal of Physics D: Applied Physics*, Vol. 40, 2008, pp. 652–662.

[26]Kotsonis, M., Ghaemi, S., Veldhuis, L., and Scarano, F., "Measurement of the body force field of plasma actuators," *Journal of Physics D: Applied Physics*, Vol. 44, 2011.

[27]Shyy, W., Jayaraman, B., and Andersson, A., "Modeling of glow discharge-induced fluid dynamics," *Journal of Applied Physics*, Vol. 92, 2002, pp. 6434–6443.

[28]Butler, K. M. and Farrell, B. F., "Three-dimensional optimal perturbations in viscous shear flow," *Physics of Fluids A*, Vol. 4, No. 8, 1992, pp. 1637–1650.